Vol. 56: 263–273, 2009
doi: 10.3354/ame01326

AQUATIC MICROBIAL ECOLOGY
Aquat Microb Ecol

Printed September 2009
Published online August 18, 2009

Contribution to AME Special 2 'Progress and perspectives in aquatic primary productivity'

OPEN ACCESS

Oxygen evolution in a hypersaline crust: *in situ* photosynthesis quantification by microelectrode profiling and use of planar optode spots in incubation chambers

Jana Woelfel[1], Ketil Sørensen[2], Mareike Warkentin[1], Stefan Forster[1], Aharon Oren[3], Rhena Schumann[1,*]

[1]University of Rostock, Institute for Biological Sciences, Albert- Einstein-Straße 3, 18059 Rostock, Germany
[2]Danish Technological Institute, Kongsrang Allé 29, 8000 Aarhus, Denmark
[3]The Institute of Life Sciences, and the Moshe Shilo Minerva Center for Marine Biogeochemistry, The Hebrew University of Jerusalem, Jerusalem, Israel

ABSTRACT: Net primary production and respiration were estimated in a hypersaline cyanobacterial mat colonizing a gypsum crust in the Eilat salterns, Israel. Two different approaches were used: *in situ* microprofiling with Clark-type O_2 sensors and application of optode sensor spots in incubation chambers. The net O_2 release rates of the mat phototrophs was high, with a maximum of 3.4 nmol O_2 cm^{-2} min^{-1} measured by microprofiling and 4.4 nmol O_2 cm^{-2} min^{-1} determined in the incubation chambers. The upper 2 layers of the mat as well as the overlying water quickly became O_2 saturated during the day. The respiration of the whole gypsum crust was also very intensive and corresponded to the O_2 produced by photosynthesis on a diurnal basis, which prevented most of the evolved O_2 from reaching the water. The results presented show that optode sensor spots are useful tools providing additional information about export and photosynthetic production rates of O_2 in hypersaline microbial mats.

KEY WORDS: Hypersaline · Gypsum crust · Microbial mat · Net production and respiration · Microelectrode · Optode

INTRODUCTION

Multi-pond solar salterns, used worldwide for salt production along the coasts in tropical and subtropical areas, are interesting environments to study limitations of marine benthic and planktonic photosynthetic processes. With a gradient of salt concentrations, from seawater to NaCl saturation, characteristic salt-adapted communities of phototrophic microorganisms can be found (Oren 2009, this Special Issue). When evaporation of seawater has proceeded to 3–4 times the original salinity (150 to 250 PSU), the solubility of calcium sulfate is exceeded and gypsum ($CaSO_4 \cdot 2H_2O$) precipitates to the bottom of the ponds and forms crusts of many centimeters thickness. Characteristically laminated communities of phototrophic microorganisms are found in these crusts: an upper layer consisting of carotenoid-rich orange-coloured *Cyanobacteria* of the *Halothece–Aphanothece* group (Garcia-Pichel et al. 1998), followed by a dark-green layer of *Phormidium*-type filamentous *Cyanobacteria* and, underneath, a purple layer of *Halochromatium* and *Ectothiorhodospira*/*Halorhodospira*, which performs anoxygenic photosynthesis with sulfide as electron donor, derived from sulfate reduction in the anaerobic layers below. The arrangement of gypsum crystals allows the light to penetrate deep into the crust, so that active photosynthesis may occur down to depths of several centimeters. Such layered phototrophic communities have been described from different salterns worldwide, e.g. in the south of France (Caumette et al.

*Corresponding author. Email: rhena.schumann@uni-rostock.de

1994), in Spain (Thomas 1984) and in Israel (Canfield et al. 2004, Sørensen et al. 2004, 2005, Ionescu et al. 2007, Oren et al. 2009).

Ambient salinity is one of the key factors determining the photosynthetic rates of the cyanobacterial community in the hypersaline gypsum crusts. A salinity decrease from 230 to 200 g l^{-1} in such a crust in Eilat increased O_2 production from <2 to 8–9 µmol O_2 l^{-1} min^{-1} as measured by a microelectrode (Canfield et al. 2004). However, our overall understanding of the photosynthetic activities in such benthic gypsum crusts and the environmental factors governing them is still extremely limited.

The measurement of benthic microbial primary production is methodologically difficult, and many different techniques have been used. The benthic O_2 exchange rate represents the most widely used proxy for quantifying respiration and primary production of marine sediments. These investigations represent a challenge in resolving variations on temporal and spatial scales covering several orders of magnitude (Glud 2008). To overcome these obstacles, O_2 sensors (electrochemical or optical) with a higher spatial and temporal resolution have been applied *in situ* to obtain O_2 profiles within sediments (e.g. Revsbech et al. 1980a, 1980b, 1983, Kühl et al. 1996), from which benthic O_2 exchange rates were then estimated. Another problem is the high degree of horizontal patchiness of the biomass as well as its activities. The latter interferes especially with O_2 profiles when using a 1-dimensional approach: the profiles are measured at a single or several distinct positions with a high vertical resolution, but the horizontal resolution within the sediment area is limited. Thus, the extrapolation of such results to larger areas (mm^2 to m^2 scale) is not always simple. Besides many *ex situ* approaches, *in situ* measurements have been carried out in benthic chambers in which primary production was estimated from the O_2 evolution over the sediment (e.g. Cahoon & Cooke 1992, Longphuirt et al. 2007, Glud et al. 2008). Such chambers integrate the patchiness corresponding to the covered sediment area, but do not resolve benthic production to the productive sediment layer(s).

O_2 microelectrodes have also been used in gypsum crusts that are difficult to penetrate, e.g. in the Salins-de-Giraud, France (Caumette et al. 1994) and in the salterns of the Israel Salt Company in Eilat (Canfield et al. 2004). Overall photosynthesis rates in the Eilat gypsum crust were much lower than those typically found in organic-rich microbial mats at lower salinities. However, on a per cell-volume basis, the rates were comparable. Benthic chambers equipped either with electrochemical sensors or optodes have rarely been applied *in situ* to gypsum crusts so far, as they cannot be drilled into the upper sediment layers to fix the chambers to the sediment surface.

Optical O_2 indicators exhibit the highest sensitivity at low O_2 concentrations and are not affected by hydrogen sulfide (Kühl & Polerecky 2008), which is often present in sediments. Furthermore, optical sensors do not consume O_2 and are thus best suited for long-term measurements at very low initial O_2 concentrations. Therefore, many studies of benthic microbial communities (e.g. reviewed in Glud et al. 1999, Kühl & Polerecky 2008) have been carried out using such optical sensor foils, ranging from µm to several cm in diameter, in combination with new imaging methods for instantaneous mapping of the distribution and dynamics of O_2 concentrations and photosynthetic activity. However, the mechanical stability of optodes in the form of sensor tips is not yet robust enough for sandy sediments and crusts. The black coating protecting the optode from scattered light is easily scratched off during profiling.

Planar O_2 optical sensor spots placed within (benthic) incubation chambers allow the determination of the export rate of O_2 from a defined sample area into the overlying water (net O_2 release). Further advantages of this approach are the easy handling and robustness under field conditions, the possibility of non-destructive sediment measurements and independence of the O_2 signal on water flow.

The aim of the present study was to quantify O_2 production and consumption in the hypersaline gypsum crust of the Eilat salterns using 2 different approaches. Net production and respiration rates calculated from micro-profiles were used to quantify organism activity (net photosynthesis) within the mat layers. However, the primary focus was net O_2 release into the overlying water as a proxy for benthic community production. The use of optode sensor spots for hypersaline and warm environments (low initial O_2 concentrations) is evaluated and the incubation chamber setup and experimental design are critically discussed. Our results demonstrate that optode sensor spots can be successfully applied to measurements of primary production in crusts under hypersaline conditions.

MATERIALS AND METHODS

Sampling site. A stable and thick gypsum crust from one pond (Pond 103) of the saltern system of Eilat, Israel, was investigated. The salterns have been in operation since 1980 and are fed with oligotrophic seawater from the Gulf of Aqaba (Eilat). Nitrate concentrations in the surface waters of the Gulf of Aqaba are <1 µmol NO_3^- l^{-1} throughout most of the year (April to November), but may increase to about 3.5 µmol NO_3^- l^{-1} at the end of the winter (Lindell & Post 1995). Phosphate concentrations are in the nM range (Stihl et al.

2001). Since 1997, brine concentrate from the seawater desalination plant in Eilat has been added to the evaporation ponds as well. Information on the types of phototrophic microorganisms in the crust studied was given by Prášil et al. (2009, this Special Issue). The rich bird life in the salterns may also add nutrients to the ponds. Average water depth in the ponds is 40 to 50 cm.

Environmental conditions. Weather data were obtained from the Israel National Monitoring of the Gulf of Eilat (www.meteo-tech.co.il). Hydrological data at sampling times are summarized in Table 1. The gypsum crusts were composed of a 5 mm orange layer at the top, followed by a second ca. 10 to 15 mm white layer, followed by a third 3 to 5 mm blue-green layer and a fourth, 2 to 3 mm thick purple layer. At the bottom of the crust, a black sediment layer was found that was not included in the *in situ* investigation of the separate layers, but which could not be excluded completely from the whole core incubations. Water content of whole cores and of each separate layer was estimated from crushed samples (for whole cores: 37 to 74 g fresh weight [FW], for separate layers: 4 to 8 g FW) as weight loss after drying.

Nutrients. Immediately after collection, water samples (ca. 50 ml) were filtered through 0.2 µm membrane filters or, in case of very mucous-rich samples, through 0.45 µm membranes, and the filtrates were kept cool at 5°C until analysis. These sterile, particle-free samples were diluted with distilled water to seawater salinity before photometric analysis. Nitrate, nitrite and phosphate were assayed using a Technicon Traacs 800 autoanalyzer. For nitrate and nitrite, we used the procedure described by Garside & Garside (1993). In addition, colorimetric analyses of ammonium, nitrite, nitrate and phosphate were performed manually. Appropriate tests were made to ensure that the salts still present did not significantly interfere with the assays, and, if necessary, corrections were made for the salt effect (Coleman & White 1993). Ammonium was assayed using the phenol-hypochlorite method developed by Solórzano (1969). Nitrate, nitrite and phosphate were assayed as outlined by Strickland & Parsons (1972).

Microelectrode profiles for net production. Intact pieces of crust (approximately 20 × 20 cm area and 10 cm deep) were sampled and transported to the laboratory, where they were incubated outside in an aquarium containing water from Pond 103 (Expt A; Tables 1 & 2). The aquarium was placed in a seawater-flooded basin that was temperature stable at 21 to 22°C. Inside the aquarium, the sides of the crust were supported by sand to preserve its shape during measurements and to prevent light from entering from the sides. Profiles were measured using Clark-type microsensors (Unisense) with guard cathodes (Revsbech 1989). Calibrations were performed in aerated brine from each pond (100% atmospheric saturation) and in a 0.1 M ascorbate + 0.1 M NaOH solution (0% oxygen) according to the manufacturer's instructions. The zero-oxygen value was also confirmed during profiling when the electrode reached the anoxic zone of the crust. The electrode was inserted in a 5 cm long and 0.8 mm thick (outer diameter) hypodermic needle (Canfield et al. 2004). Profiles were measured every 30 min in the morning from 5:30 to 10:30 and in the afternoon from 16:00 to 19:00. The sensor required about 30 s to equilibrate at each new depth, and it took approximately 15 min to measure each profile. To decrease the risk of breaking the sensors, 3 to 4 successive profiles were measured in the same location instead of moving the sensor before each new profile. The measurements were thus performed in a total of 4 different locations (Table 2). The sensors were controlled using a micromanipulator and a PC-controlled motor unit. Data collected from the picoamperometer were continuously collected on the PC using Sensor Trace PRO v1.9 software (Unisense). Diffusive vertical

Table 1. Environmental conditions during the experiments on gypsum crust O_2 evolution: density of the brine in g cm^{-3}, water temperature, nutrients (a: ammonium, n: nitrate, p: phosphate) and average daily solar radiation. Incubation water for experiments was taken during sampling, from the filtered water used for the incubations, and from the respective experiments: (A) O_2 profiles on intact crusts; (B1) O_2 evolution of separate layers without nutrient enrichment and (B2) with nutrient enrichment; (C1) daily O_2 evolution over whole cores of crusts at *in situ* solar radiation and (C2) partly shaded

Date	Brine density	Water temperature (°C)	Nutrients (µmol l^{-1})	Solar radiation (W m^{-2})	Samples
01 April	1.106	28		298	Gypsum crust
02 April				303	Gypsum crust
03 April	1.109		a: 0–0.5	306	Incubation water
			n: 3.1–4.6		
			p: 3.3–3.9		B1, C1
04 April				253	A
05 April				289	B2, C2

Table 2. Treatments and microprofiles for each experiment

Expt	Description	Light conditions	Samples/treatments	No. of replicates
A	*In situ* microprofiles	Morning and evening solar radiation	15 profiles measured in 4 consecutive holes	n.d.
B1	Net O_2 export under *in situ* solar radiation	7 intervals over 24 h (total 40 h)	1	3
B2	Net O_2 export of fully exposed and shaded cores	5 intervals over 24 h (total 29 h)	2	2 for each treatment
C1	O_2 production of all 4 separate layers	1 dark and 4 light steps	4	n.d.
C2	O_2 production of orange and blue-green layers with N and NP additions	1 dark and 3 light steps	4	n.d.

fluxes of O_2 across the crust–water interface were estimated using Fick's first law of diffusion

$$J = -\Phi \times D \times \mathrm{d}C/\mathrm{d}x \quad (1)$$

In Eq. (1), J is the net diffusive flux, Φ is the tortuosity, D is the diffusion coefficient of O_2 in the crust, which depends on salinity, temperature and porosity, and $\mathrm{d}C/\mathrm{d}x$ is the concentration gradient of O_2 with depth. O_2 fluxes were estimated from the O_2 concentration gradient in the boundary layer at and immediately above the crust surface. Here, effects from tortuosity and porosity are negligible and the diffusion coefficient equals that of water at the same temperature and salinity. The distribution of O_2 in the crust was measured at different times during the day. The net O_2 diffusion across the crust–water interface was estimated from each of the measured profiles using Eq. (1). The net rate of O_2 accumulation in the crust was calculated by estimating and comparing the total O_2 content of the crust at different times, accounting for a porosity of 0.5 and based on the depth-integrated concentration profiles. Furthermore, net O_2 production was estimated as the sum of accumulation in the crust and upward flux across the interface. Downward O_2 flux into the crust was neglected as downward concentration gradients were generally lower than upward gradients. Porosity (~0.5) and tortuosity in the crust would additionally decrease downward fluxes calculated to <25% of the net O_2 diffusion across the interface.

O_2 measurements with planar optode spots. The planar O_2 sensor spots (∅: 5 mm) (PreSens) were glued to the inner walls of the incubation chambers. Molecular oxygen quenches the luminescence of the dye immobilized in the O_2-permeable matrix of the sensor spots. This fluorescence signal decrease was measured non-invasively by a 1 m (for separate layers) or a 10 m (for whole core measurements) long glass fiber through the Plexiglas wall of the chamber. The measuring accuracy of planar sensor spots is around ± 0.5% at 85.0 µmol O_2 l^{-1} and ± 5% at 2.8 µmol O_2 l^{-1} (PreSens, cited in Warkentin et al. 2007, p. 6724).

Since the conversion matrix of the measured signal into saturation and concentration was not applicable for salinities >40 PSU, the signal was calibrated against the chemical volumetric determination of O_2 concentration (Winkler 1888) in 164 PSU (1.109 g O_2 ml^{-1}) water with the help of the Stern-Volmer relationship.

$$\frac{I_f^0}{I_f} = 1 + k_q \tau_0 \cdot [Q] \quad (2)$$

In Eq. (2), I^0_f is the intensity of fluorescence without a quencher, I_f is the intensity of fluorescence with a quencher, k_q is the quencher rate co-efficient, τ_0 is the fluorescence lifetime of the dye without a quencher present and [Q] is the concentration of the quencher. From that, we calculated the factor ($k_q \cdot \tau_0$) by fitting concentrations against phases (Fig. 1). This factor and maximal phase I^0_f were used to convert all later optode measurements into O_2 concentrations.

Up to 20 min of initial data were omitted from the analyses or not recorded because of phase changes

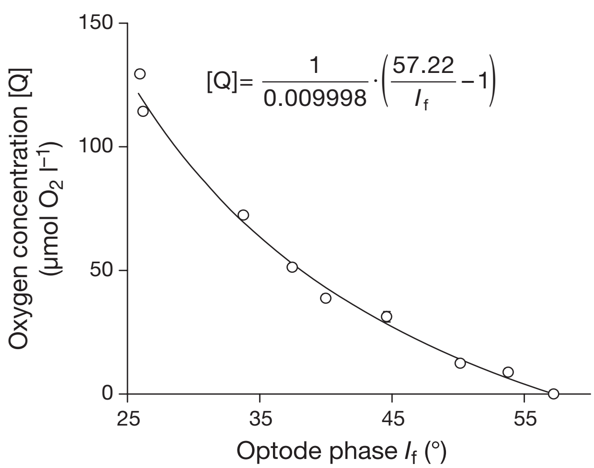

Fig. 1. Oxygen concentration (µmol l^{-1}) as determined by Winkler titration and optode phase signal (°) in NaCl solutions (164 PSU) of different oxygen saturations provided by nitrogen bubbling at 21°C. Trend from fitting concentrations [Q] against phases I_f after the Stern-Volmer equation (Eq. 2) (factor of 0.009998 is $k_q \times \tau_0$ and I^0_f = 57.22)

between sample and the spot and/or chamber due to temperature equilibration. The release rates were calculated from the decrease or increase of O_2 in the supernatant water volume during dark (called respiration) and light treatments (benthic O_2 release or, in case of separate layers, net production). These rates were converted into fluxes driven by the core or layer areas or chl *a* contents, respectively. The conversion of O_2 into C units was done with a factor of 1 (1 C per 1 O_2), assuming carbohydrate to be the main photosynthesis product.

Incubation setup to determine net O_2 export of specific layers. Two methodological approaches, both based on planar O_2 sensor spots, were used to determine net O_2 export of (1) whole crust cores and (2) separate layers of the microbial mat (Table 2). For (1), the spots (1 per core) were situated in the upper part of 3 replicate chambers, approximately at a distance of 10 to 11 cm from each other. For (2), the spots (1 per layer) were positioned at 2 cm distance to each sectioned layer in 4 replicate chambers. All chambers were filled completely with water from Pond 103, from which O_2 oversaturation was removed by bubbling with N_2, and sealed air-tight.

For (1), net O_2 release over >24 h was recorded from whole cores cut from crusts sampled on 1 April and exposed to *in situ* irradiation at constant temperature conditions (21 to 22°C) on 3 and 5 April (Expts B1 & B2). Up to three replicate air-tight plexiglass incubation chambers (185 mm height, inner diameter 40 mm, 232.5 ml) with whole cores contained a 3 cm magnetic stirring cross, which mixed potential O_2 gradients in the water column for 10 min prior to O_2 readings. The stirring cross rotated at 6 to 7 rpm and was driven by an external rotating magnet. We frequently noticed the accumulation of bubbles at the mat surface within the core tubes. After stirring, most bubbles disappeared from the water phase. The chambers were enveloped in dark foil up to the top 2 to 5 mm of the crust to avoid irradiation of the core sides. Approximately 10 manual readings were taken per measurement with an average deviation of 2.1%.

For (2) (Expts C1 & C2), cores from the same gypsum crust were sliced into 4 layers using a knife and spatula, and measured separately. The top orange layer was obtained as one piece (approximately an ellipse of 30 × 35 mm) and the 3 other layers (white, blue-green and purple) broke down into ca. 5 to 10 mm pieces of gypsum crystals with attached microorganisms. All pieces were transferred immediately into plexiglass incubation chambers (40 mm inner diameter, 50 mm height, 62.8 ml). The intact top layer was up to 10 mm thick and the gypsum particles formed several mm deep layers. Layer volume was estimated and included as reference parameter. Gas bubbles attached to the gypsum particles were removed with a spatula and only bubble free samples were incubated.

All chambers (Expts B1, B2, C1 & C2) were pre-incubated in a 26°C water bath in darkness for a minimum of 1 h, which was close to the *in situ* temperature. After that, a dark incubation period of 3 to 3.5 h was started, during which O_2 concentrations in the 4 incubation chambers were read at least twice over a time span of >10 min. After that, up to 4 different light treatments were applied. All O_2 measurements were taken over a duration of ca. 10 min, providing O_2 values every 5 s. The lowest photon flux (PFD) of 20 µmol photons m^{-2} s^{-1} was achieved by shading the fluorescent lamps (Philipps TLD 15W 54) with 3 layers of black gauze, and PFDs of 30, 40 and 80 µmol photons m^{-2} s^{-1} were obtained by 2 or 1 layer(s) of gauze or without shading, respectively. Nutrients [3 µM phosphate (+P) or 3 µM phosphate and 48 µM nitrate (+NP)] were added in a follow-up experiment, in which only the third (blue-green) phototrophic layer was investigated.

Biomass parameters. Chlorophyll *a* (chl *a*) was extracted with 90% acetone (12 h in darkness at 5°C) from ca. 0.5 to 2 g wet weight (ww) of homogenized crust particles retrieved from the incubation chambers after the O_2 measurements. Afterwards, the centrifuged supernatant was determined according to Jeffrey & Humphrey (1975) except for the blank absorption, which had to be measured at 850 nm due to interference by bacteriochlorophylls at 750 nm (Oren et al. 1995). The deviation of chl *a* per g ww of crust for triplicate extractions per sample was highest in the orange layer (14 to 109%), because the gypsum particles were rather large (up to 7 mm) and hard to homogenize. The other layers and whole cores had a better reproducibility with an average of 33 and 14%, respectively. For the estimation of the total organic carbon (TOC) concentration and the molar ratio of carbon to nitrogen (C:N ratio) within the crust, ca. 150 mg of dry material were measured (after inorganic carbon was expelled with a 10% HCl solution) in an element analyzer (Vario EL, Elementar) according to Verardo et al. (1990).

RESULTS

Environmental conditions

Pond 103 had a salinity of 157 to 164 PSU and a water temperature of ca. 28°C in the afternoon when samples were collected. Nitrate and phosphate concentrations in the water overlaying the crust were 3 to 5 µmol NO_3^- l^{-1} and 3 to 4 µmol PO_4^+ l^{-1}, respectively (Table 1). Average daily solar radiation was 285 W m^{-2} in late March/early April. While whole core incubations

(Expts B1 & B2) on 3 and 5 April were carried out on days with this average radiation, which is based on almost cloud-free days, *in situ* microprofiling (Expt A) was carried out on a day with radiation levels ca. 10% below average, due to many hours of cloud cover during the incubation.

Microbial biomass in the gypsum crusts

Whole cores had a water content of 20 to 26%. The TOC content was rather low with 0.16 to 0.20% of dry mass. The blue-green (third) layer was the only one with an organic carbon content slightly above average with up to 0.28% of dry mass. The molar C:N ratio was 7.5 to 8.9 within the 4 upper separate layers, while the 2 phototrophic layers (first: orange; third: blue-green) had values at the upper end of range. In whole cores including a black-grey (fifth) layer, molar C:N ratios of 6.3 to 9.5 according to Hillebrand (1999) did not indicate a severe nitrogen limitation of the microphytobenthos either. Chl *a* contents increased with depth from 0.7–1.9 to 7.5–11 µg g dry weight^{-1} in the purple (fourth) layer. The high amount of chl *a* in the purple layer may only partly be attributed to material derived from the green layer above, since much care was taken to avoid contamination when separating the layers. Instead, it may have been derived from degrading inactive cyanobacterial biomass.

Net O_2 production within the crust

Fig. 2 shows examples of O_2 profiles measured in the crust from Pond 103. There was a small peak of O_2 at about 3 mm in the profile from 05:30 am, indicating that respiration during the night did not entirely exhaust the pool of O_2 generated during the day. Primary production commenced at sunrise, and the net flux across the crust–water interface as estimated from the measured O_2 release at the surface (Eq. 1; Table 3) was reversed 1 h later. Estimated exchange rates reached about 0.06 nmol O_2 cm^{-2} s^{-1} around noon and decreased during the afternoon. At sunset, the estimated flux was again close to zero. The net rates of O_2 accumulation within the crust in the morning and O_2 consumption in the afternoon were generally at least an order of magnitude higher than the estimated rates of diffusion across the crust–water interface (Table 3), indicating that a large proportion of the O_2 produced by *Cyanobacteria* in the orange and green layers was retained and consumed within the crust. The profiles indicated that O_2 diffused at a rate of about 0.008 nmol O_2 cm^{-2} s^{-1} from the water phase into the upper ca. 2 mm of the crust during the night.

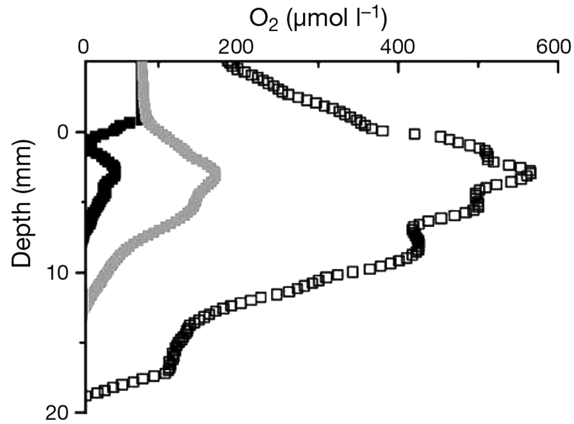

Fig. 2. Oxygen profile in a crust from Pond 103 measured in the morning on 4 April. Measurements taken at (■) 05:30, (■) 06:30, (□) 09:30

O_2 release from whole cores and production in separate layers

Incubations of whole cores started in the early evening hours at O_2 concentrations of 83 to 103 µmol O_2 l^{-1} in the supernatant water (Fig. 3). During the night, O_2 decreased to almost a quarter of the initial concentration in the water phase in some chambers. While O_2 concentrations were still very low at 11:00 am, they started to increase around 12:00 and reached maxima of ca. 122 µmol O_2 l^{-1} late in the afternoon, ca. 24 h after incubations started. Calculating changes in O_2 concentration from one measuring time to the next, maximum respira-

Table 3. O_2 content, O_2 release (O_2 exchange) rate, and net O_2 production calculated from microprofiles measured on 4–5 April 2008. O_2 content is the depth-integrated O_2 profile, accounting for porosity (0.5 vol/vol), from the crust–water interface down to the O_2 depletion depth; O_2 exchange rate was calculated from the O_2 gradient in the boundary layer neglecting porosity and tortuosity; net O_2 production = O_2 content + O_2 exchange rate

Time	O_2 content (nmol cm^{-2})	O_2 release rate (nmol cm^{-2} s^{-1})	Net O_2 production (nmol cm^{-2} s^{-1})
05:30	139	−0.008	
06:00	322	−0.001	0.10
06:30	673	0.004	0.20
07:00	1238	0.007	0.32
07:30	1936	0.018	0.41
08:00	2153	0.016	0.14
08:30	2476	0.018	0.20
09:00	3053	0.016	0.34
09:30	3250	0.018	0.13
10:30	3360	0.057	0.09
16:00	2099	0.048	−0.02
16:30	1631	0.023	−0.24
17:20	1176	0.026	−0.13
18:00	1106	0.007	−0.02
19:00	397	0.010	−0.19

tion rates were –0.056 nmol O_2 cm^{-2} s^{-1} at night and maximum net release rates were +0.074 nmol O_2 cm^{-2} s^{-1} during the day (Fig. 4). Although the supernatant water was only saturated (100% ≈105 µmol l^{-1} at 21°C) for a few hours during late afternoon, gas bubbles developed at or reached the sediment surface, where they may have caused an underestimation of gas exchange at the sediment–water interface. In a follow-up experiment (Expt B2), in which 2 whole cores were again exposed to full and another 2 to ca. 50% *in situ* radiation, similar O_2 production rates were recorded in all 4 samples, indicating that light is not a limiting factor for O_2 release over the sediment–water interface (see also Figs. 3 & 4). Since the cores used in Expt B1 had rather high pigment concentrations, the biomass-related maximum release rates were very low with 0.11 to 0.25 mg C mg chl a^{-1} h^{-1}.

Respiration rates of separate gypsum layers ranged from –0.003 to –0.031 nmol O_2 cm^{-2} s^{-1}, which is at the lower range of the values calculated from the microprofiles. The upper orange layer had the highest O_2 demand (Fig. 5). Although PFDs were comparatively low at 40 µmol photons m^{-2} s^{-1}, the 2 layers dominated by *Cyanobacteria* (upper orange and third blue-green layer) reached positive net production rates of 0.019 and 0.011 nmol O_2 cm^{-2} s^{-1}, respectively (Fig. 6). The maximum production rate, measured at 80 µmol photons m^{-2} s^{-1}, which was the highest possible radiation to be reached with the illumination equipment used, was 0.041 nmol O_2 cm^{-2} s^{-1}. This corresponded to ca. 55% of the maximum rates measured in whole cores during full daylight. In the 2 other layers (white and purple), O_2 concentrations also decreased continuously under increasing PFDs, and positive net production rates were never determined. In a follow-up experiment (not shown), the 2 productive layers (orange and blue-green) were enriched with nutrients. Respiration rates were slightly higher with –0.003 to –0.068 nmol O_2 cm^{-2} s^{-1} and O_2 export started at 80 µmol photons m^{-2} s^{-1}. Biomass-related production rates of all photosynthetic layers amounted to 0.02 to 0.33 mg C mg chl a^{-1} h^{-1}.

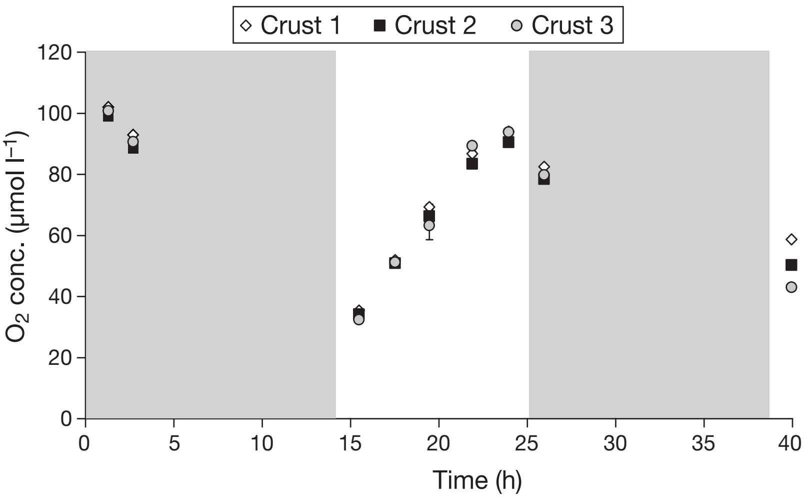

Fig. 3. Oxygen concentration (µmol l^{-1}) in Pond 103 cores at 12 to 15 cm^2 and 5 to 6 cm depth under natural solar radiation at 22°C on 3 April (grey: night hours)

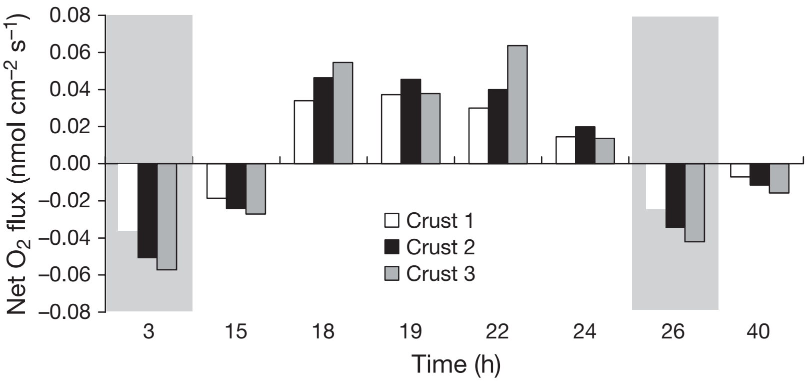

Fig. 4. Net oxygen flux (nmol O_2 cm^{-2} s^{-1}) over the water–sediment interface calculated from data presented in Fig. 3 (grey: night hours)

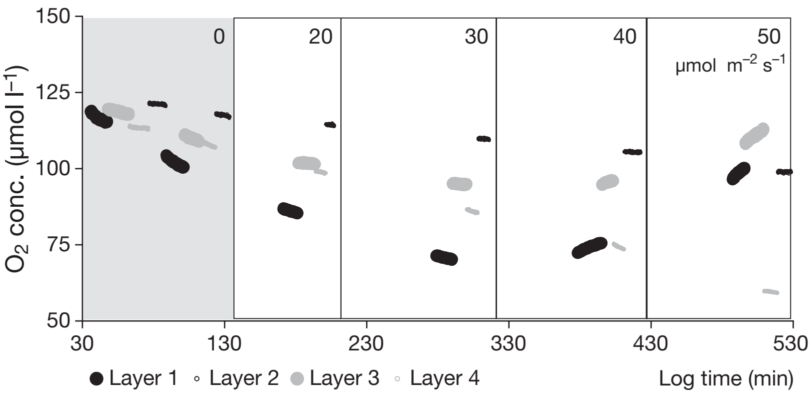

Fig. 5. Development of O_2 concentration (µmol l^{-1}) on 3 April in 4 separate layers from Pond 103 crust, submersed in ca. 60 ml habitat water, under different photon fluxes (0, 20, 30, 40 and 80 µmol photons m^{-2} s^{-1}). 1: orange layer, dominated by *Aphanothece/Halothece*; 2: white layer, rich in mucilage; 3: blue-green layer, dominated by filamentous *Cyanobacteria*; 4: purple layer, dominated by purple sulfur bacteria

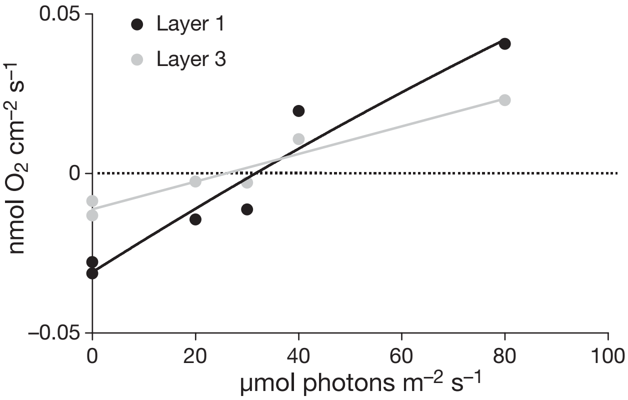

Fig. 6. Net O_2 flux (nmol O_2 cm^{-2} s^{-1}) in relation to photon flux (µmol photons m^{-2} s^{-1}) in 2 separate autotrophic layers submersed in 50 ml habitat water, calculated from data presented in Fig. 5. 1: *Aphanothece*/*Halothece*; 3: filamentous *Cyanobacteria*

DISCUSSION

Microbial community of the gypsum crusts

The distribution pattern of photosynthetic microorganisms in the mats observed in the salterns of Eilat (Oren et al. 1995, Prášil et al. 2009) was similar to those reported for other mats found in hypersaline environments, e.g. Salins-de-Giraud, France (Caumette et al. 1994) and Guerrero Negro on the Pacific coast of Baja California, Mexico (Rothschild et al. 1994). The occurrence of the (second) white layer is sometimes explained by a local nutrient depletion, where the orange-brown layer absorbs nutrients from the overlying water and the green layer obtains its nutrients from anaerobic degradation processes in the lower layers (Oren et al. 2009). It is unlikely that, in the crusts studied by us, nitrogen was a limiting nutrient because many of the *Cyanobacteria* present, including some strains of *Aphanothece*/*Halothece*, may have fixed N_2 (Kohl & Niklisch 1988). P limitation, in contrast, was indicated by a high phosphatase activity visualised by ELF-Phosphate hydrolysis (cf. Sirová et al. 2006) in the gypsum crusts (data not shown).

The low organic carbon content of the Eilat mats was surprising, because the microbial consortia were so dense that they colored 3 of the 4 layers by their species-specific pigments. The second (white) layer was heavily loaded with mucous material leaking from the severed margins in several centimeters long strands. Thus, the low organic carbon content must be attributable to the large (and heavy) gypsum particles, which do not allow for a large surface area on which microorganisms can settle. Furthermore, the water content of whole cores was low at ca. 20% and similar to that of medium grain size sandy sediments (Woelfel et al. 2007). Thus, comparisons to other sediments, which are based on sediment mass parameters, are biased. Compared to marine subtidal sediments at a water depth of 0 to 1 m (cf. Cahoon 1999 and references therein, Woelfel et al. 2007), the pigment content of 56 to 577 mg chl *a* m^{-2} of the microbial mats in the Eilat gypsum crusts was rather high. Studies from laminated microbial mats (9 mm depth) of other saltern ponds, e.g. Guerrero Negro (Mexico), found much higher concentrations of 430 to 2040 mg chl *a* m^{-2} (Palmisano et al. 1989). The specific architecture of the crusts allows for considerable biomass colonising deeper layers while receiving sufficient amounts of light. In the upper layers of the crust, scalar irradiance reached up to 200% of the incident irradiance at the crust surface due to intense scattering (Oren et al. 1995). Even where chl *a* was found at comparable depths in sandy or silty marine sediments, the O_2 evolution was—unlike in the gypsum crusts—usually restricted to the upper 5 mm because of poor light penetration and a high light absorption by the microphytobenthos living on top of the sediment (Cohen 1989).

O_2 production and exchange via the crust surface

The estimated net O_2 release based on *in situ* microprofiling were in the same range as those obtained by whole core incubations. Differences between the 2 approaches were conspicuous especially during morning measurements. Although negative O_2 net production rates were measured in the optode-equipped chambers, positive rates were determined by the microsensor within the mat. It is possible that a small amount of H_2S present in the overlying water in the *in situ* set up had to be chemically reduced first. In a previous report from Pond 200, O_2 release rates, based on estimated molecular diffusion from microprofiling, were also consistent with results of benthic chamber incubations (Canfield et al. 2004). Since the amount of available data is very limited and the general problems with spatial heterogeneity mentioned above are considerable, further comparisons of the net O_2 release rates measured using the 2 setups are of little relevance.

The rates of dark (night) O_2 release measured using the 2 methods differed substantially, with rates of 0.008 nmol cm^{-2} s^{-1} estimated from microprofiles and 0.056 nmol cm^{-2} s^{-1} from the whole core incubations. Based on previous evidence from other ponds in the Eilat salterns (Canfield et al. 2004), the estimated rate obtained with the microsensor appears to be very low in the present study. This may also be attributed to spatial heterogeneity, so that more measurements at several other crusts and core incubations will yield a better and more conclusive overview on net O_2 release rates during the day and at night.

Measured microprofiles showed that most of the O_2 generated during the day did not escape the crust (Table 3). Both the present and previous studies on the Eilat salterns have indicated that most of the O_2 produced in the third (green) layer is retained and consumed within this layer and, therefore, O_2 supersaturation does not occur (Canfield et al. 2004). Furthermore, due to O_2 consumption by the oxidation of metal sulfides accumulated during the dark period (Wieland et al. 2005), measurements of O_2 release rates alone may cause an important underestimation of the net O_2 production rate. However, H_2S gradients simultaneously measured in the crusts of Pond 103 do not support substantial chemical O_2 consumption (Sørensen et al. 2009, this Special Issue). This is interesting from a mass-balance perspective, since it indicates that most of the organic material generated during daytime is already consumed by the following morning. O_2 profiles measured during day/night cycles in microbial mats of the Guerrero Negro evaporation ponds (salinity 0.65 to 1.25 mg ml^{-1}) have also shown that, during daytime, most of the O_2 formed in the mat is recycled locally by respiration of organic carbon (Canfield & Des Marais 1993). At night, oxidation of sulfide near the mat–water interface was the main O_2-consuming process; thus, dissimilatory sulfate reduction is the principal source of dissolved inorganic carbon (DIC) at night. In the Eilat crust, 30% of the O_2 produced during the first half of the light cycle accumulated in the crust (Canfield et al. 2004), compared to less than 1% in Guerrero Negro, Baja California Sur, Mexico (Canfield & Des Marais 1993, Des Marais 1995). A careful comparison of the O_2 and DIC fluxes across the crust–water interface revealed that, during the day, more inorganic carbon diffuses into the mat than O_2 diffuses out (Oren 2009).

The net O_2 production rates in the photoautotrophic zones, measured by optode sensor spots, were rather low with 1.4 nmol O_2 cm^{-2} min^{-1} in the orange and 2.5 nmol O_2 cm^{-2} min^{-1} in the green layer (cf. Table 1 in Oren 2009). This may be attributed partly to the maximum photon flux of 80 µmol photons m^{-2} s^{-1} applied, an intensity insufficient for maximum net photosynthesis (Fig. 6). In the whole cores of the *in situ* approach, higher net O_2 release rates of 4.4 nmol O_2 cm^{-2} min^{-1} were determined, which are comparable to the net production rate of up to 10.8 nmol O_2 cm^{-2} min^{-1} measured by Wieland et al. (2005) in the Salins de Giraud, France. This indicates that such exchange rates and, therefore, the laminated mat or crust communities strongly depend on high solar radiation levels. It still remains to be evaluated if and to what extent O_2 exchange rates reflect carbon fixation (and biomass growth) when other O_2 depletion processes are very high.

Applicability of the benthic chamber setup

Availability of O_2 in hypersaline waters is limited due to the low solubility of O_2, which is further diminished by the ambient high temperatures (Sherwood et al. 1991, 1992). Additionally, the O_2 release rates, i.e. the net O_2 production of the sediment, may be low. Thus, O_2 measurements with optodes are recommended for low concentration-change rates. The principle of (benthic) incubation chambers equipped with sensor spots allows a simple determination of O_2 exchange over whole cores or net production in slurries without subsampling (Winkler) or chemical O_2 consumption (Clark electrodes). Biofilm formation on the spots has not been observed so far, and if it should occur, the spots are easy to clean chemically or by autoclaving. The spots are fairly resistant to drying and have had a long lifetime in our laboratory so far. However, the absence of O_2 gradients in the chambers remains to be checked carefully. The chamber approach opens many further possibilities to manipulate whole sediment cores or slurries and to estimate production rates under more controlled radiation conditions. Most often, the respective biomass parameters are available (in contrast to microprofile approaches), e.g. chl *a* per area, volume or sediment mass, from which microphytobenthos productivity, e.g. as O_2 evolution per biomass unit, can be estimated. O_2 productivity per biomass unit is a valuable parameter to compare different microphytobenthic communities. Of course, extrapolation of such results to *in situ* conditions must be done with great care.

Acknowledgements. This study was carried out during the 8th International Workshop of Group for Aquatic Primary Productivity (GAP) and Batsheva de Rothschild Seminar on Gross and Net Primary Productivity held at the Interuniversity Institute for Marine Sciences, Eilat, Israel in April 2008. We thank the Batsheva de Rothschild Foundation, Bar Ilan University, the Moshe Shilo Center for Marine Biogeochemistry, and the staff of the Interuniversity Institute for funding and logistic support. Further financial support was also received from the Deutsche Forschungsgemeinschaft (Schu 965/7-1, Wa 2723/1-1) and the FAZIT Foundation (for J.W.). We also thank the Israel Salt Company in Eilat, Israel for allowing access to the salterns.

LITERATURE CITED

Cahoon LB (1999) The role of benthic microalgae in neritic ecosystems. Oceanogr Mar Biol 37:47–86

Cahoon LB, Cooke JE (1992) Benthic microalgal production in Onslow Bay, North-Carolina, USA. Mar Ecol Prog Ser 84: 185–196

Canfield DE, Des Marais DJ (1993) Biogeochemical cycles of carbon, sulfur, and free oxygen in a microbial mat. Geochim Cosmochim Acta 57:3971–3984

Canfield DE, Sørensen K, Oren A (2004) Biogeochemistry of a gypsum-encrusted microbial ecosystem. Geobiology 2: 133–150

Caumette P, Matheron R, Raymond N, Relexans JC (1994) Microbial mats in the hypersaline ponds of Mediterranean Salterns (Salins-De-Giraud, France). FEMS Microbiol Ecol 13:273–286

Cohen Y (1989) Photosynthesis in cyanobacterial mats and its relation to the sulfur cycle: a model for microbial sulfur interactions. In: Cohen Y, Rosenberg E (eds) Microbial mats: physiological ecology of benthic microbial communities. Am Soc Microbiol, Washington DC, p 22–36

Coleman MU, White MA (1993) The role of biological disturbances in the production of solar salt. In: Kahihana H, Hardy HR Jr, Toyikura K (eds) Seventh symposium on salt, Vol I. Elsevier, Amsterdam p 623–631

Des Marais DJ (1995) The biogeochemistry of hypersaline microbial mats. In: Jones JG (ed) Advances in microbial ecology, Vol. 14. Plenum Press, New York, p 251–274

Garcia-Pichel F, Nübel U, Muyzer G (1998) The phylogeny of unicellular, extremely halotolerant *Cyanobacteria*. Arch Microbiol 169:469–482

Garside C, Garside JC (1993) The '*f*-ratio on 20°W during the North Atlantic Bloom Experiment. Deep-Sea Res 2:75–90

Glud RN (2008) Oxygen dynamics of marine sediments. Mar Biol Res 4:243–289

Glud RN, Kühl M, Kohls O, Ramsing NB (1999) Heterogeneity of oxygen production and consumption in a photosynthetic microbial mat as studied by planar optodes. J Phycol 35:270–279

Glud RN, Eyre BD, Patten N (2008) Biogeochemical responses to mass coral spawning at the Great Barrier Reef: effects on respiration and primary production. Limnol Oceanogr 53:1014–1024

Hillebrand H (1999) Effects of biotic interactions on the structure of microphytobenthos. PhD Thesis, University of Kiel

Ionescu D, Lipski A, Altendorf K, Oren A (2007) Characterization of the endoevaporitic microbial communities in a hypersaline gypsum crust by fatty acid analysis. Hydrobiologia 576:15–26

Jeffrey SW, Humphrey GF (1975) New spectrophotometric equations for determining chlorophylls *a, b,* c_1 and c_2 in higher plants, algae and natural phytoplankton. Biochem Physiol Pflanz 167:191–194

Kohl JG, Niklisch A (1988) Ökophysiologie der Algen. Wachstum und Ressourcennutzung. Akademie-Berlag, Berlin

Kühl M, Polerecky L (2008) Functional and structural imaging of phototrophic microbial communities and symbioses. Aquat Microb Ecol 53:99–118

Kühl M, Glud RN, Ploug H, Ramsing NB (1996) Microenvironmental control of photosynthesis and photosynthesis-coupled respiration in an epilithic cyanobacterial biofilm. J Phycol 32:799–812

Lindell D, Post AF (1995) Ultraphytoplankton succession is triggered by deep winter mixing in the Gulf of Aqaba (Eilat), Red Sea. Limnol Oceanogr 40:1130–1141

Longphuirt SN, Clavier J, Grall J, Chauvaud L and others (2007) Primary production and spatial distribution of subtidal microphytobenthos in a temperate coastal system, the Bay of Brest, France. Estuar Coast Shelf Sci 74: 367–380

Oren A (2009) Saltern evaporation ponds as model systems for the study of primary production processes under hypersaline conditions. Aquat Microb Ecol 56:193–204

Oren A, Kühl M, Karsten U (1995) An endoevaporitic microbial mat within a gypsum crust: zonation of phototrophs, photopigments, and light penetration. Mar Ecol Prog Ser 128:151–159

Oren A, Sørensen KB, Canfield DE, Teske AP, Ionescu D, Lipski A, Altendorf K (2009) Microbial communities and processes within a hypersaline gypsum crust in a saltern evaporation pond (Eilat, Israel). Hydrobiologia 626:15–26

Palmisano AC, Cronin SE, Amelio E, Munoz E, Des Marais D (1989) Distribution and survival of lipophilic pigments in a laminated microbial mat community near Guerrero Negro, Mexico. In: Cohen Y, Rosenberg E (eds) Microbial mats, physiological ecology of benthic microbial communities. American Society for Microbiology, Washington, DC, p 138–152

Prášil O, Bína D, Medová H, Řeháková K, Zapomělová E, Veselá J, Oren A (2009) Emission spectroscopy and kinetic fluorometry studies of phototrophic microbial communities along a salinity gradient in solar saltern evaporation ponds of Eilat, Israel. Aquat Microb Ecol 56: 285–296

Revsbech NP (1989) An oxygen sensor with a guard cathode. Limnol Oceanogr 24:474–478

Revsbech NP, Sørensen J, Blackburn TH, Lomholt JP (1980a) Distribution of oxygen in marine sediments measured with microelectrodes. Limnol Oceanogr 25:403–411

Revsbech NP, Jørgensen BB, Blackburn TH (1980b) Oxygen in the sea bottom measured with a microelectrode. Science 207:1355–1356

Revsbech NP, Jørgensen BB, Blackburn TH, Cohen Y (1983) Microelectrode studies of the photosynthesis and O_2, H_2S, and pH profiles of a microbial mat. Limnol Oceanogr 28:1062–1074

Rothschild LJ, Giver LJ, White MR, Mancinelli RL (1994) Metabolic activity of microorganisms in gypsum-halite crusts. J Phycol 30:431–438

Sherwood JR, Stagnitti F, Kokkinn MJ, Williams WD (1991) Dissolved oxygen concentrations in hypersaline waters. Limnol Oceanogr 36:235–250

Sherwood JR, Stagnitti F, Kokkinn MJ, Williams WD (1992) A standard table for predicting equilibrium dissolved oxygen concentrations in salt lakes dominated by sodium chloride. Int J Salt Lake Res 1:1–6

Sirová D, Vrba J, Rejmánková E (2006) Extracellular enzyme activities in benthic cyanobacterial mats: comparison between nutrient-enriched and control sites in marshes of northern Belize. Aquat Microb Ecol 44:11–20

Solórzano L (1969) Determination of ammonia in natural waters by the phenol hypochlorite method. Limnol Oceanogr 14: 799–801

Sørensen K, Řeháková K, Zapomělová E, Oren A (2009) Distribution of benthic phototrophs, sulfate reducers, and methanogens in two adjacent saltern evaporation ponds in Eilat, Israel. Aquat Microb Ecol 56:275–284

Sørensen KB, Canfield DE, Oren A (2004) Salt responses of benthic microbial communities in a solar saltern (Eilat, Israel). Appl Environ Microbiol 70:1608–1616

Sørensen KB, Canfield DE, Teske AP, Oren A (2005) Community composition of a hypersaline endoevaporitic microbial mat. Appl Environ Microbiol 71:7352–7365

Stihl A, Sommer U, Post AF (2001) Alkaline phosphatase activities among populations of the colony-forming diazotrophic cyanobacterium *Trichodesmium* spp. (Cyanobacteria) in the Red Sea. J Phycol 37:310–317

Strickland JD, Parsons TR (1972) A practical handbook of seawater analysis, 2nd Ed. Bull Fish Res Board Canada 167

Thomas JC (1984) Formations benthiques à Cyanobactéries des salins de Santa Pola (Espagne): Composition spécifique, morphologie et caractéristiques biologiques des principaux peuplements. Rev Inv Geol 38/39: 139–158

Verardo DJ, Froelich PN, McIntyre A (1990) Determination of organic carbon and nitrogen in marine sediments using the Carlo Erba NA-1500 Analyser. Deep-Sea Res 37: 157–165

Warkentin M, Freese HM, Karsten U, Schumann R (2007) New and fast method to quantify plankton community respiration by optical oxygen sensor spots. Appl Environ Microbiol 73:6722–6729

Wieland A, Zopfi J, Benthien M, Kühl M (2005) Biogeochemistry of an iron-rich hypersaline microbial mat (Camargue, France). Microb Ecol 49:34–49

Winkler LW (1888) The determination of dissolved oxygen in water. Ber Deutsch Chem Gesell 21:2843–2855

Woelfel J, Schumann R, Adler S, Hübener T, Karsten U (2007) Diatoms inhabiting a wind flat of the Baltic Sea: Species diversity and seasonal succession. Estuar Coast Shelf Sci 75:296–307

Editorial responsibility: Ilana Berman-Frank, Ramat Gan, Israel

Submitted: December 1, 2008; Accepted: May 14, 2009
Proofs received from author(s): July 20, 2009